Available online at www.sciencedirect.com
SCIENCE DIRECT®
Journal of Molecular Catalysis A: Chemical 216 (2004) 263–272
JOURNAL OF MOLECULAR CATALYSIS A: CHEMICAL
www.elsevier.com/locate/molcata

Step dynamics and step–step interactions on the chiral Cu(5 8 90) surface

Margret Giesen*, Sabine Dieluweit

Forschungszentrum Jülich, Institut für Biologische Schichten ISG 4, D 52425 Jülich, Germany

Abstract

In this paper we discuss particular aspects of the high-Miller-index Cu(5 8 90) surface. We focus on the mobility of steps and energetic step–step interactions and the possible influence of kink–kink interactions on the step structure. One important goal of this paper is to give a detailed insight into the characteristics of a typical real high-Miller-index surface, such surfaces are frequently used as substrates in enantioselective reactions because of their chiral surface properties.

Keywords: High-Miller-index; Step dynamics; Step–step interaction

1. Introduction

Since the pioneering work on the reactivity and adsorption of gases on high-Miller-index surfaces in the early seventies by the Somorjai and co-workers [1–3] and by Perdereau and Rhead [4], stepped and kinked surfaces have attracted some scientific interest. Some of the experimental studies focused on the structure and stability of high-Miller-index surfaces during adsorption [5–8]; others investigated surface reconstructions [9–13] or surface relaxations [14]. The importance of high-Miller-index surfaces (or "vicinal" surfaces as they are frequently called) in surface science was acknowledged by introducing a special notation such that the structure of the denoted crystal planes could be recognized straight forwardly just by their notation (sometimes denoted as the "Somorjai notation") [15].

In all of the experimental studies mentioned so far, merely the static surface structure of vicinal surfaces was considered. Triggered by the invention of scanning probe microscopy techniques [16,17] and the possibility to obtain real-space images of solid surfaces, steps and kinks were more and more recognized as mobile defects which are present also on low-Miller-index crystal facets due to thermal excitation. For vicinal surfaces, it was found that the thermal excitation of steps and kinks may lead to a new phase transition below the melting point of a facet, the so-called "roughening transition" [18,19]. Above the roughening transition, the mean square height correlation function of a facet diverges due to the thermal excitation of steps and kinks. For one-dimensional defects such as steps the corresponding mean square deviation function [20,21] diverges for any temperature $T > 0$ K, i.e. steps are always rough above absolute zero temperature. (This result has important consequences for two-dimensional crystals, i.e. islands, which never reveal straight facet edges but have always rounded island edges [22], and according to the Wulff-construction [23], the anisotropic step free energy cannot have cusps.) In thermodynamic equilibrium, all surfaces have (according to the respective formation energies) a defined equilibrium concentration of thermally activated steps, kinks and other defects such as terrace adatoms and vacancies. On vicinal surfaces with a high density of geometric steps and kinks due to the azimuthal and polar angles, the number of thermal kinks, and in particular steps, may be negligible at low temperature. At higher temperatures, however, they may have a considerable effect on the surface structure. The ranges of "low" and "high" temperatures are first determined by the cohesive energy of the material. Diffusion and activation barriers are known to roughly scale with the cohesive energy, i.e. the higher the cohesive energy, the higher are the diffusion and activation barriers. Then, higher temperatures are required to excite

* Corresponding author. Tel.: +49-2461-614108; fax: +49-2461-613907.
E-mail address: m.giesen@fz.juelich.de (M. Giesen).

1381-1169/$ – see front matter © 2004 Elsevier B.V. All rights reserved.
doi:10.1016/j.molcata.2004.03.027

thermal kinks, for instance. Secondly, the orientation of the crystal plane determines the range of low and high temperatures. Cu(1 1 *n*) surfaces (*n* an odd number) are vicinal to the (0 0 1) plane and the steps are oriented parallel to the atomically dense ⟨1 1 0⟩-direction. Here, thermally excited kinks play a significant role already around room temperature [24,25]. This is in contrast to Cu(5 8 90): This surface plane is vicinal to (0 0 1), however, the steps are oriented off the atomically dense ⟨1 1 0⟩-direction and the concentration of geometric kinks is 0.23. For this surface, the excitation of a comparable amount of thermal kinks would require a surface temperature of about 625 K [26].

In thermodynamic equilibrium, the step and kink structure of high-Miller-index surfaces is not static but undergoes fluctuations due to the mobility of kinks and step edges. Kink diffusion along steps is caused by the evaporation of atoms from kink sites or the capture of atoms at kinks. As a consequence, the step profile changes permanently due to atomic processes at the step edges. The mobility of steps on metal as well as on semiconductor surfaces has been investigated in numerous studies since the early nineties (for recent reviews see [20,21]). From the specific time-dependence of the step fluctuations one may determine the dominant atomic transport mechanism responsible for the step mobility. By means of temperature-variable investigations, formation energies of kinks and steps as well as activation barriers for atomic transport at steps can be determined with high accuracy.

The importance of high-Miller-index surfaces and the relevance of their natural chirality [27] for enantioselective chemical reactions have been considered only very recently [28–31]. Most, the effect of thermal excitation of steps and kinks on the enantioselectivity of platinum vicinal surfaces has been taken into account [32,33]. These studies, however, represent merely a first step towards the understanding of real high-Miller-index surfaces and their interaction with chiral molecules. Two important aspects and their consequences for the enantioselectivity of stepped surfaces which were neglected so far are the interaction between steps and the effect of adsorbates on the step morphology. When prepared under ultra-high vacuum (UHV) conditions, most vicinal surfaces tend to form regular arrays of terraces separated by steps of one atomic height. This morphology is stabilized by an elastic step–step repulsion which is inversely proportional to the square of the step–step distance (for reviews see [20,21]). The larger the elastic repulsive interaction, the narrower is the terrace width distribution (TWD). These repulsive interactions stabilize the surface against an agglomeration of steps in certain areas of the surface (“step-bunching”). While regular step arrays are stable for most vicinal surfaces prepared in UHV, an interaction with adsorbates may cause step-doubling [34] or step-bunching [35–38]. A similar observation is made when vicinal metal surfaces are in electrochemical environments. Frequently, the formation of step pairs are observed and in the course of thermal equilibrium fluctuations the surface eventually separates into areas of large terraces and bunched steps [39,40].

In this paper we discuss, as an example, results on the step mobility and step–step interactions of the high-Miller-index Cu(5 8 90) surface. We discuss the influence of kinks and steps on the spatial and time fluctuations of steps and on the step–step interactions as well as the possible contribution of kink–kink interactions to the energetics of high-Miller-index surfaces.

The paper is organized as follows. Section 2 describes the experimental set-up and gives some general remarks on the measuring principles. In Section 3, the experimental results are presented. They will be discussed in Section 4 and the paper ends with a brief summary in Section 5.

2. Experimental set-up, measuring principles and geometrical aspects of chiral surfaces

The experiments were performed in a standard ultra-high vacuum chamber equipped with a temperature-variable microscope [41,42] with high thermal drift stability. The tunneling tip is made from polycrystalline tungsten wire. Typical tunneling parameters used in the experiments are a tunneling current of 1–1.5 nA and a tunneling bias of 0.3 V. The STM were recorded in the constant-current mode with a pixel resolution of 512 × 512. Typical times to scan an image were 40–60 s. These parameters are known to have no measurable influence on atomic diffusion processes at copper steps [21]. For the experiments we used copper surfaces with the Miller indices (5 8 90). The surface normal of this crystallographic plane is rotated by 5.98° with respect to the normal of the (0 0 1) plane. The resulting monatomic steps on the surface are rotated with respect to the atomically dense ⟨1 1 0⟩-direction by nominal 12.99° which corresponds to a density of geometric kinks of 0.23 per nearest-neighbor distance along the atomically dense ⟨1 1 0⟩-direction. The samples were cut from a single crystal rod with (1 0 0)-orientation by spark erosion. They were polished and oriented by diffractometry to the desired orientation within 0.1°. The accuracy is limited by the natural mosaic structure of the single crystal. Prior to mounting the samples in the chamber they were annealed to 900 °C in an (1:25) H:Ar atmosphere for 2 h. After this procedure, most of the natural sulphur content in a copper crystal rod is leached and even after prolonged heating in the UHV chamber to 700 °C no sulphur is detected in the Auger spectrum. There is, however, still sulphur contamination visible in the STM images. To get rid of this sulphur and to remove the oxygen layer, the samples were furthermore cleaned after the bake-out of the UHV chamber by repeated cycles of 5×10^{-5} mbar Ne sputtering and subsequent annealing to 700 °C. Since sulphur segregation from the bulk to the surface layer region starts around 500 °C, the crystal was annealed at a maximum temperature of 400 °C in the last annealing cycle such that the surface was kept free of sulphur. After that procedure, the sample surfaces revealed clean and well-oriented, parallel steps, which display on

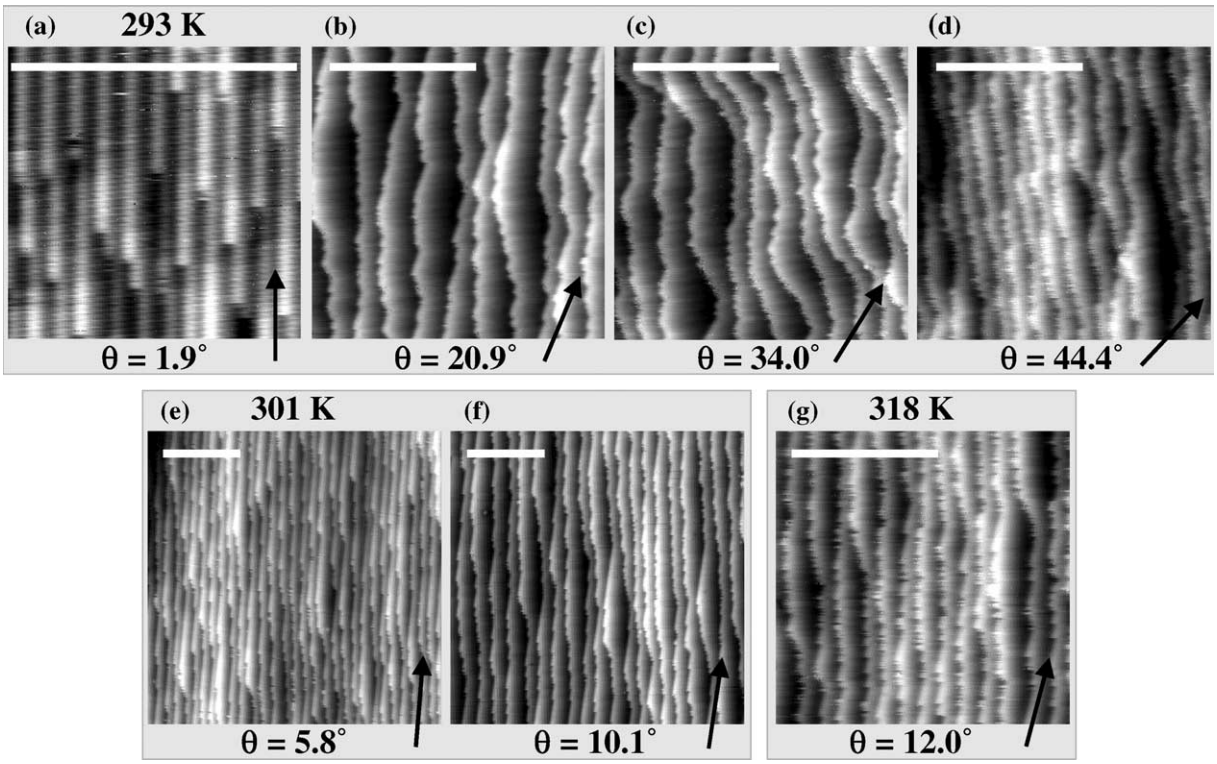

Fig. 1. STM images of various areas on a Cu(5 8 90) sample. Locally, the angle θ between the mean orientation of the steps and the atomically dense ⟨1 1 0⟩-direction (indicated by a black arrow), and hence the kink concentration, may vary substantially. Due to atomic motion at the step edges, the steps may appear frizzy. The step frizziness becomes dominant in particular for large θ or higher temperatures. The white bar in each image indicates a length of 10 nm.

average the nominal rotation angle of 12.99° of the (5 8 90) surface. The misalignment of the steps with respect to the ⟨1 1 0⟩-direction varied locally between 0 and 45°. The size of the local area of constant angle was of the order of 10^4 nm^2. Fig. 1 shows STM images of different areas on the Cu(5 8 90) surface with various mean step orientations with respect to ⟨1 1 0⟩, i.e. with different concentrations of forced kinks and at three different temperatures. The mean rotation angle of the steps was determined by averaging over all steps in an image. The straight step segments between kink sites are oriented along the atomically densely packed ⟨1 1 0⟩-direction (black solid arrows in Fig. 1(a)–(g)) which was determined by a crystallographic marker on the sample and could be precisely related to the chosen scan direction during image recording. Depending on the angle between the mean step orientation and the ⟨1 1 0⟩-direction, the step edge profile contains different numbers of kink sites. In Fig. 1(d), for instance, the kink density is almost 100% ($\theta = 44.4°$) and the step profile is close to a zig–zag pattern. In some areas, the steps were rotated by more than 45°. Hence, the geometric kinks at these steps revealed the mirror symmetry compared to kinks at steps with angles between 0 and 45°. (If one denotes the latter as "right-handed" kinks, the former would be "left-handed" kinks.) Fig. 2 shows microscopic models which display possible step profiles for various kink concentrations. Which of the possible step profiles is realized on a given surface depends on the energy balance of step, kink and corner formation energies.

To acquire a sufficiently large data base for the analysis of the step fluctuations and the terrace width distribution we first searched for an area with a distinct step orientation on the sample and then recorded 10–20 images such that we could analyze about 100 steps with a total length of 1–2 μm. After that, we searched for another surface area with different step orientation and proceeded as before.

In our experiments, we used two different recording modes of our STM. First, for the analysis of the terrace width distribution we recorded normal, so-called "spatial" STM images or "*x*–*y*-scan" where the STM tip scans over a square shaped surface area, i.e. the coordinates *x*, *y* perpendicular and along the steps are spatial coordinates. These images were also used in our previous work [43] where we studied the step stiffness on Cu(5 8 90). Second, for the analysis of the time fluctuations we recorded so-called "time lapse images" or "*x*–*t*-scan" where the tip repetitively scans the same line perpendicular to the steps. The individual lines are displayed in a pseudo image in which y is replaced by a time axis. Fig. 3 shows (a) a spatial STM image of the Cu(5 8 90) surface at 301 K and (b) the corresponding time lapse image composed from the top most scan line in (a). In the time lapse image, the typical step profile generated by geometric kinks is not visible any more. "Kink-like" structures as observed in (b) are caused by kinks (geometric

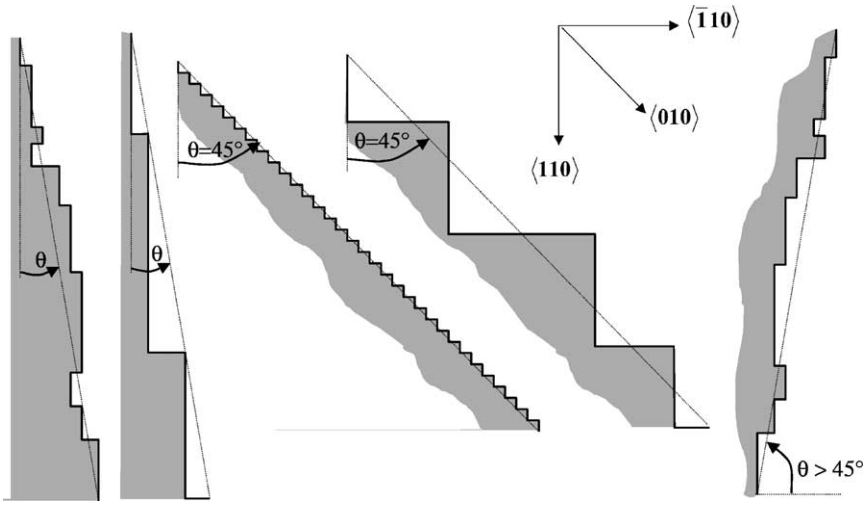

Fig. 2. Depending on the energetics of the material, nominally identical high-Miller-index surfaces may reveal very different step and surface structures. The step profile may contain regularly distributed kinks or may consist of one-dimensional facets, i.e. step segments oriented along the densely packed atomic crystallographic directions. Which of the possible step profiles is realized on a given surface depends on the energy balance of step, kink and corner formation energies. One should emphasize that locally even step orientations with angles larger than 45° are possible. In this case, the steps reveal locally a majority of kinks with mirror symmetry compared to the geometrically ideal kinks of a nominal high-Miller-index surface.

or thermally activated kinks) moving across the scan line during image recording which gives rise to sudden jumps in the step position by one row. The resulting "rough" appearance of the step edges as seen in the time lapse image in Fig. 3(b) has been denoted as "frizziness" [24–26,44]. We should emphasize though, that the step frizziness is also observed in normal spatial STM images (Fig. 3(a)): Depending on the relevant diffusion barriers, sample temperature and scan speed, kink motion may be much faster than the time to scan a line during STM recording. Then, a normal *x*–*y*-scan includes a superposition of spatial and time information, in particular in the slow *y*-scan direction, or may even be dominated by the time information such that the *y*-direction represents, in fact, a time axis [45].

For the final analysis of the STM images, we determined first the mean rotation angle of the steps with respect to the ⟨1 1 0⟩-direction by averaging over all steps in the particular image. In our measurements we chose the scan directions

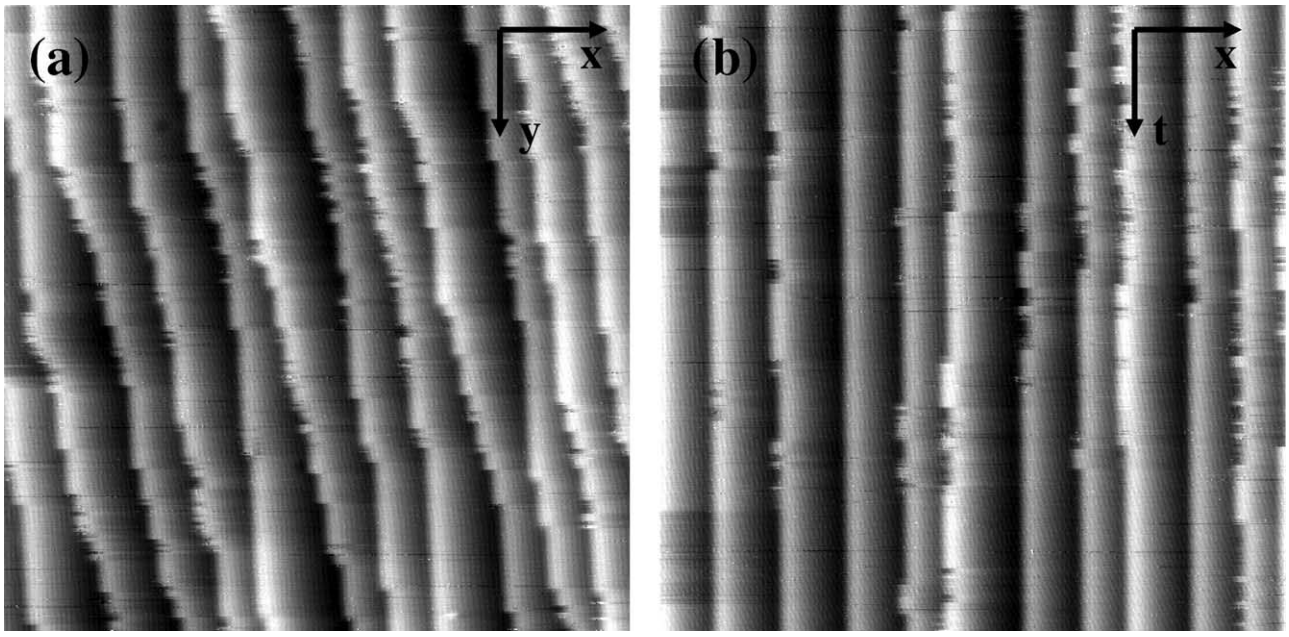

Fig. 3. (a) "Normal" (spatial) STM image of a surface area of the Cu(5 8 90) sample at $T = 301$ K. Scan area 24.3 nm × 24.3 nm. (b) Corresponding time lapse image composed from the top most scan line in (a). The axis perpendicular to the apparent steps is a normal spatial axis (scan width 24.3 nm), the axis parallel to the apparent step edges is a time axis (total time for 512 lines 57 s).

such that the mean orientation of the steps was roughly oriented from the top to the bottom border of the STM images.

3. Results

3.1. Time fluctuations and influence of kinks on step edge diffusion

Time fluctuations of steps in equilibrium are analyzed by means of a time correlation function [24,26,45,46]

$$G(t) = \langle (x(t) - x(t_0))^2 \rangle = c(T,\theta) L^{\delta} (t - t_0)^{\alpha} \quad (1)$$

in which $c(T,\theta)$ is a temperature- and angle-dependent prefactor (with θ the rotation angle between the step orientation and the $\langle 1\,1\,0 \rangle$-zone axis) containing all activation energies for surface mass transport at steps. L is the mean distance between steps and the exponents α and δ may assume values 1/4, 1/3, 1/2 depending on the dominant mass transport causing the step fluctuations [47–52]. For $\alpha = 1/4$ and $\delta = 0$, the dominant mass transport is diffusion of atoms and kinks along the step edge, and the step correlation function is [53]

$$G(t) \approx 0.464 \left[\frac{k_B T}{\tilde{\beta}(\theta) a_{||}} \right]^{3/4} (\Gamma_h)^{1/4} t^{1/4} \quad (2)$$

where $\tilde{\beta}(\theta)$ is the step stiffness, $a_{||}$ the nearest-neighbor atomic distance and Γ_h is the hopping coefficient [53].

The angle dependent stiffness $\tilde{\beta}(\theta)$ can be determined from a spatial correlation function (obtained from purely spatial STM images)

$$G(y) = \langle (x(y) - x(y_0))^2 \rangle = \frac{k_B T}{\tilde{\beta}(\theta) a_{||}} |y - y_0| a_{||} \quad (3)$$

The factor $k_B T/\tilde{\beta} a_{||}$ has been determined in a previous study [43]. For convenience, the result is reproduced in Fig. 4. $\tilde{\beta}(\theta)$ can also be determined from the analysis of the equilibrium shape of islands [22] and the result is plotted in Fig. 4 as black diamonds. For further discussion we refer to [43]. It should be emphasized that the dependence of the spatial step profile on the kink concentration cannot be described by a simple next-nearest-neighbor model [43]. Rather higher-order kink–kink interactions must be taken into account.

Fig. 5(a) and (b) show time correlation functions $G(t)$ (Eq. (1)) for $T = 293$ and 318 K and various values of θ in a log–log plot. In such a plot, $G(t)$ is linear within the scattering. Fig. 5(c) displays the time exponents deduced from $G(t)$ as shown in Fig. 5(a) and (b) for temperatures between 293 and 328 K and various values of θ. The time exponents determined from the time correlation functions lie between 0.13 and 0.52; the average value is $\bar{\alpha} = 0.33 \pm 0.03$.

For Cu(0 0 1) at 360 K, the time exponents are $\bar{\alpha} = 0.25$ [25], and hence, the dominant mass transport is diffusion along the steps. As we will discuss in detail in Section 4.1,

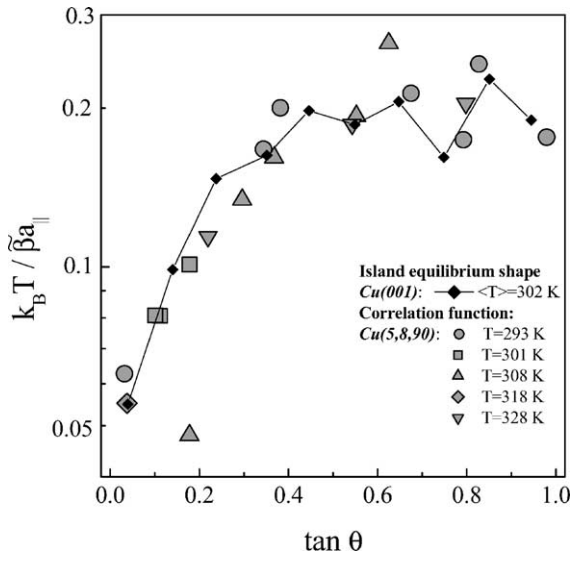

Fig. 4. The normalized inverse step stiffness $\tilde{\beta}$ vs. the angle of the step with respect to the atomically dense $\langle 1\,1\,0 \rangle$-direction. $\theta = 0$ corresponds to 0% geometric kinks (kinks at steps are thermally activated) and $\theta = 45^{\circ}$ corresponds to 100% (geometrically) kinked step edges [43].

it is reasonable to assume also that for Cu(5 8 90), edge diffusion is the dominant mass transport process. For further analysis of the experimental data, we make use of the respective theoretical equations for the case of dominant edge diffusion, i.e. Eq. (2), in the following.

From the temperature variable data we may also determine the activation energy and the pre-exponential factor of the hopping coefficient Γ_h by rewriting Eq. (2) and plotting $G(t)$ for $t = 1$ s

$$\frac{[G(t = 1s)]^4}{(0.464)^4 (k_B T/\tilde{\beta}(\theta) a_{||})^3} \approx \Gamma_h = \Gamma_0 e^{-E_{\Gamma_h}/k_B T} \quad (4)$$

in an Arrhenius-plot. For the plot displayed in Fig. 6 we used the experimental data for $k_B T/\tilde{\beta}(\theta) a_{||}$ as shown in Fig. 4 [43]. The data points for a distinct value of θ stem from experiments performed at different temperatures. As was demonstrated in [43], the variation of $k_B T/\tilde{\beta}(\theta) a_{||}$ in the temperature range of interest here is negligible for $\theta > 5^{\circ}$ since the concentration of geometric kinks is much larger than the concentration of thermally activated kinks. Note, however, that for the data in Fig. 6 for $\theta \approx 2^{\circ}$, the temperature dependence of $k_B T/\tilde{\beta}(\theta) a_{||}$ is not negligible.

From Fig. 6 one finds that Γ_h decreases with increasing θ up to about $\theta = 20^{\circ}$ and saturates for larger values of θ. Although the number of data points is small it is obvious that the activation energy of Γ_h is approximately independent of θ. Due to the small number of data points we cannot safely determine an angle-dependence of the pre-factor Γ_0. Γ_0 has large error bars and hence we have determined an average value for the pre-exponential factor as well as for the activation energy in Fig. 7. In addition, we have included data points (open and solid stars) stemming from previous experiments [45,46] performed on Cu(1 1 n) vicinal surfaces

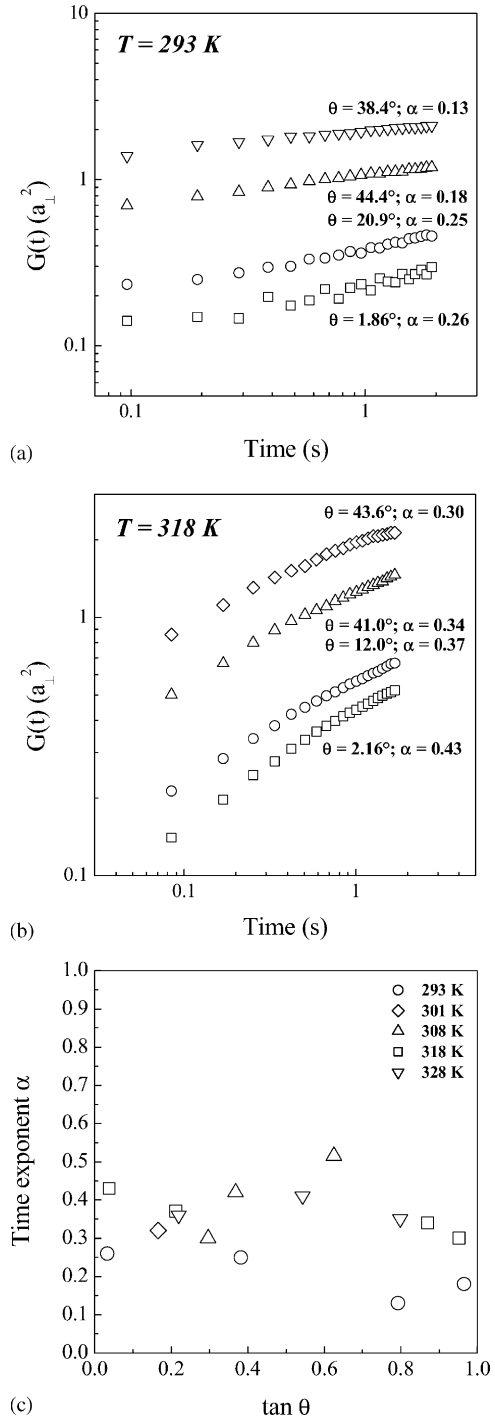

Fig. 5. $G(t)$ as measured at (a) $T = 293\,\mathrm{K}$ and (b) $T = 318\,\mathrm{K}$ for various step misorientation angles θ. (c) Measured time exponents α vs. $\tan\theta$ for all temperatures.

where the steps on average are oriented along the atomically dense $\langle 1\,1\,0\rangle$-direction. Since for small but finite θ, the temperature dependence of $k_\mathrm{B}T/\tilde{\beta}(\theta)a_{||}$ is not negligible due to thermally activated kinks, we have not plotted the results for $\theta \approx 2^\circ$ in Fig. 7. The mean value of the activation energy E_{Γ_h} is $0.68 \pm 0.12\,\mathrm{eV}$. For the pre-exponential factor we find a mean value of $\Gamma_0 = 2.8 \times 10^{21}\,\mathrm{s}^{-1}$. Due to the small

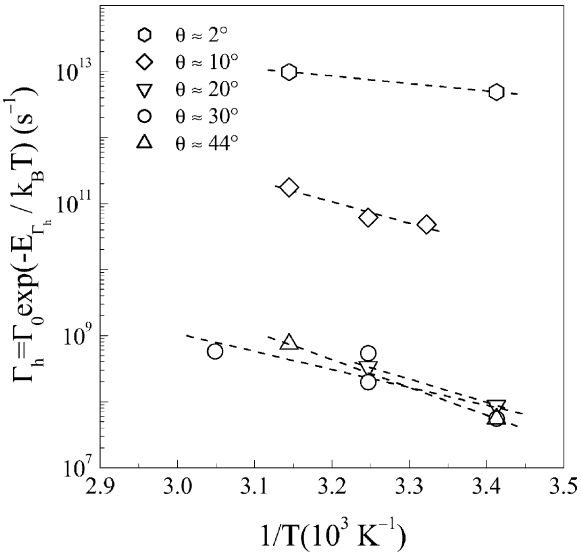

Fig. 6. Arrhenius plot of the hopping coefficient Γ_h (Eqs. (2) and (4)) for various step angles θ (see text for details).

number of data points the results for the activation energy and the pre-exponential factor of Γ_h should be interpreted as approximate values, respectively, as an indicator of the order of magnitude.

3.2. Step–step interactions and terrace width distribution

As has been shown in quite a number of publications (for details see [20,21] and references therein) the terrace width distribution may be described in a mean-field approximation in terms of a Gaussian [20,21]

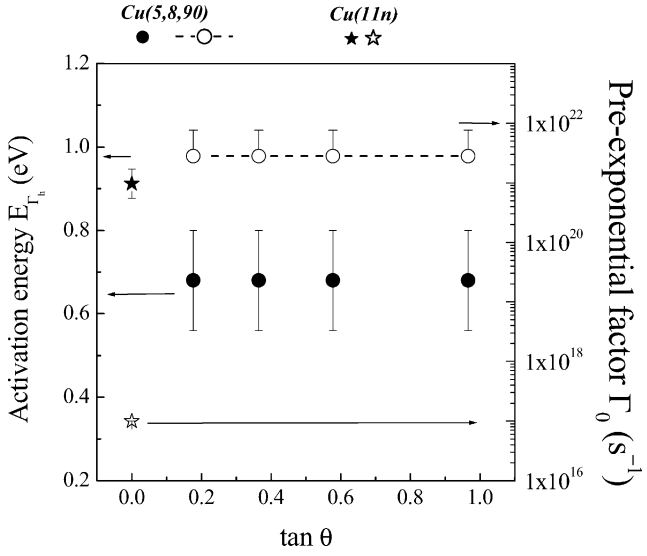

Fig. 7. Angle-dependence of the pre-exponential factor Γ_0 (open circles) and the activation energy E_{Γ_h} (solid circles) of the hopping coefficient Γ_h (Eq. (4)). For comparison, at $\theta = 0$ (open and solid star) previous data for the pre-exponential factor and the respective activation energy for steps parallel to $\langle 1\,1\,0\rangle$ are plotted (data taken from [25]).

$$P(s) = \frac{1}{\sigma_G\sqrt{2\pi}}\exp\left\{-\frac{(s-1)^2}{2\sigma_G^2}\right\} \quad (5)$$

Here, $P(s)$ is the probability to find steps in a distance s, where $s = x/\langle L\rangle$ ($\langle L\rangle$ the mean terrace width). The Gaussian width σ_G of the distribution is given by

$$\sigma_G^4 = \frac{1}{48\tilde{\beta}A_G} \quad (6)$$

where A_G is the step–step interaction constant. Eq. (6) is a good approximation for TWDs with small skewness [54]. Hence, by measuring TWDs and the corresponding Gaussian width, one may determine the step–step interaction constant between steps if the step stiffness is known.

In order to study the angle dependence of the step–step interaction constant we have measured the TWDs on Cu(5 8 90) at different temperatures and for $0 < \theta < 45^\circ$. Fig. 8 shows TWDs obtained at $T = 293$ K for different values of θ as circles. The data is normalized to the local value of the mean terrace width. Represented by the solid curves are the Gaussian fits which obviously are in good agreement with the experimental data.

We have also measured TWDs for 301, 308 and 318 K for various misorientation angles θ. From this data we obtained the angle- and temperature-dependent Gaussian width and the interaction constant A_G according to Eq. (6), which are shown in Fig. 9(a) and (b), respectively. We find that the Gaussian width reveals no obvious dependence on θ within the error bars and that the interaction constant slightly increases with tan θ.

4. Discussion

4.1. Angle-dependence of step edge diffusion

First, we want to discuss our results with respect to the dominant mass transport at the steps on Cu(5 8 90). It was previously shown that the dominant mass transport around room temperature is edge diffusion for vicinal surfaces to Cu(1 0 0) with steps along ⟨1 1 0⟩ [25]. In that case, the time exponent is $\alpha = 0.25$. It was also shown that the theoretical value for α is assumed only for large fluctuations (i.e. $G(t)/a_\perp^2 \gg 1$). If $G(t)/a_\perp^2 < 1$, one may find exponents around 1/3 and even up to 1/2. This is easily understood, because for low kink concentrations, $G(t)$ may be derived in the limit of non-interacting kinks where step fluctuations are best described by a random walk of kinks which yields $\alpha = 1/2$. In that case, atom motion is essentially along straight

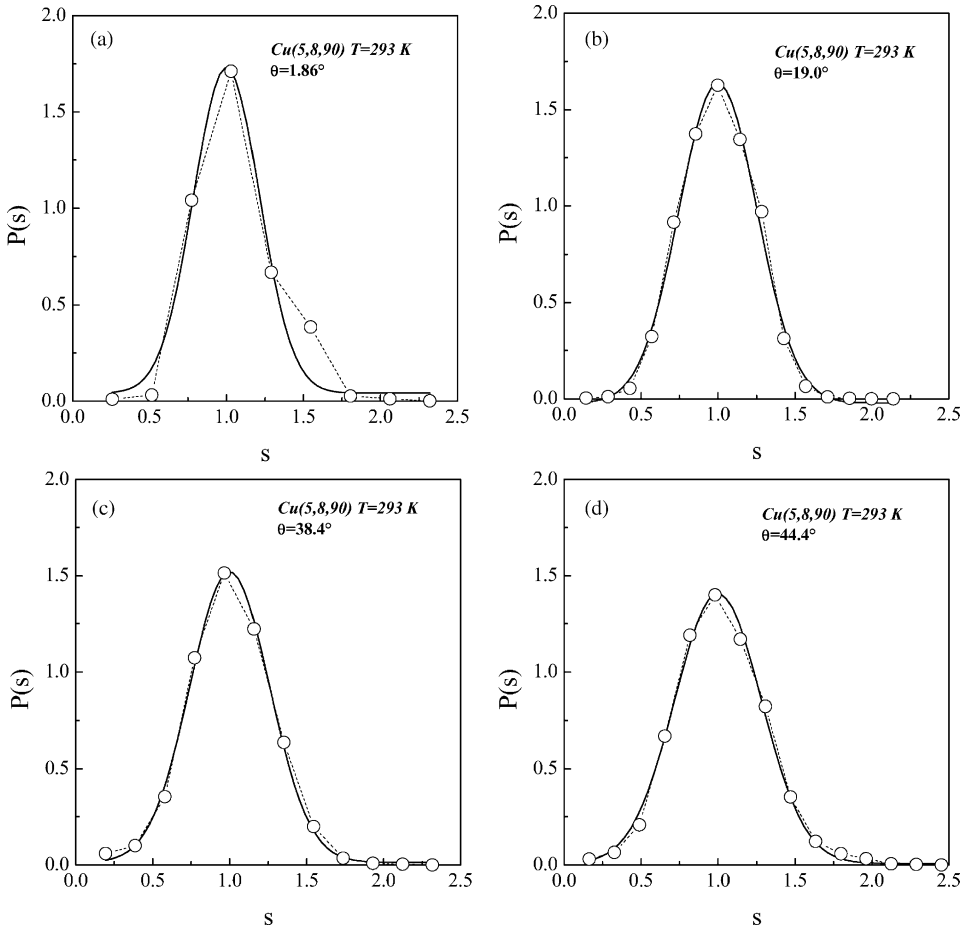

Fig. 8. TWDs for Cu(5 8 90) at $T = 293$ K and for various angles θ (open symbols). The solid lines are fits to a Gaussian according to Eq. (6).

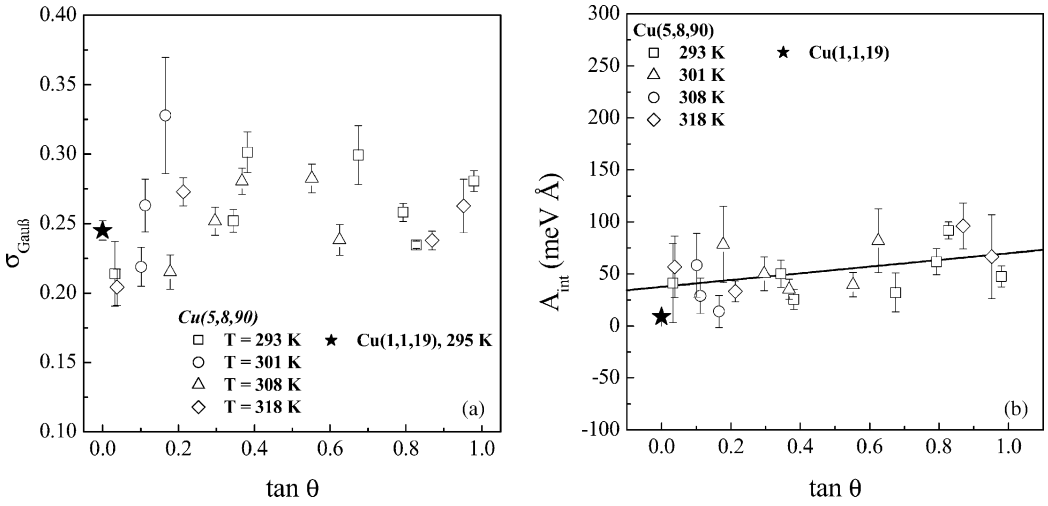

Fig. 9. (a) Gaussian width σ_G as determined from all measured TWDs. (b) Interaction constant A_G vs. $\tan\theta$ obtained using Eq. (6) (open symbols). The temperatures corresponding to these data points are indicated. The gray star represents a previous result obtained for steps on Cu(1 1 19) oriented along ⟨1 1 0⟩ [54].

sections of the step. Since $G(t)$ for our data is still well below 1 we cannot safely determine the relevant time exponent. A similar problem arose in earlier studies of Cu(1 1 n) surfaces on which steps have no geometric kinks [25]. Here, $G(t)/a_\perp^2$ was below 1 for $T < 340$ K and the time exponents assumed values between 0.30 and 0.40. Around 360 K, however, $G(t)/a_\perp^2$ was larger than 1 and the respective time exponent was 0.25, indicative of preferred edge diffusion. Therefore, it is reasonable to assume that the dominant mass transport on Cu(5 8 90) in the considered temperature regime between 293 and 328 K is also step edge diffusion. This assumption is confirmed by the data shown in Fig. 5(b). Here, the exponent decreases systematically from α close to 1/2 to a value close to 1/4 with increasing θ, i.e. with increasing kink concentration.

We may furthermore compare the temperature dependence of $G(t)$ as measured here with previous data for Cu(1 1 n) vicinal surfaces [25]. From Fig. 7 we find that the activation energy obtained for Cu(1 1 n) ($E_{\Gamma_h} = 0.91$ eV) is larger than for Cu(5 8 90) (mean value $E_{\Gamma_h} = 0.68 \pm 0.12$ eV). For Cu(0 0 1), the activation barrier was determined in a temperature range, where $G(t)/a_\perp^2 > 1$, and hence, a considerable amount of atom motion involves diffusion around kinks. In the case of Cu(5 8 90) in the temperature range up to 328 K, we propose that diffusion around kinks is negligible. Hence, the measured activation barrier of $E_{\Gamma_h} = 0.68$ eV solely would represent adatom creation from kinks and diffusion of adatoms along straight step sections. The larger activation barrier of $E_{\Gamma_h} = 0.91$ eV as measured earlier for Cu(0 0 1) could therefore be indicative of a kink–Ehrlich–Schwoebel barrier as discussed by Pierre-Louis et al. [57]. A kink–Ehrlich–Schwoebel barrier is the one-dimensional analog to the Ehrlich–Schwoebel step edge barrier [55,56], which is an additional energy barrier for atoms crossing step edges. The kink–Ehrlich–Schwoebel barrier for diffusion around kinks would cause additional energy contributions to the diffusion barrier along kinked steps. In this case, one would expect E_{Γ_h} to depend on the misorientation angle for Cu(5 8 90) when $G(t)/a_\perp^2 > 1$. In order to measure an angle-dependence of E_{Γ_h}, one would have to extend the temperature regime to higher values. This could not be performed on Cu(5 8 90) due to the small mean step–step distance on this vicinal surface: At temperatures above 318 K the step fluctuations were considerably restricted due to step–step interactions. In order to study the effect of a possible kink–Ehrlich–Schwoebel barrier for large fluctuations, the experiments would have to be performed on a sample with lower step density.

A further striking result is that the surprisingly large pre-exponential factor of $10^{17\pm2}\,s^{-1}$ as obtained for Cu(1 1 n) [45,46] is confirmed by the studies on Cu(5 8 90) presented here. Even if one considers the large uncertainty of Γ_0 as measured for Cu(5 8 90) the pre-exponential factor seems to be slightly larger compared to Cu(1 1 n).

4.2. Step–step interaction constant

As becomes obvious from Fig. 9(a), the Gaussian widths of the terrace width distributions as observed for the Cu(5 8 90) surface show no obvious angle-dependence. The step–step interaction constant, on the other hand, reveals a slight dependence on the concentration of geometric kinks (Fig. 9(b)). The only study on the step–step interaction constant of kinked steps on copper surfaces the authors are aware of was published by Rousset et al. [58]. Our results may be compared with their data, the direct comparison, however, is not very helpful: Rousset et al. studied the TWD on Cu(8 1 0) which is vicinal to Cu(0 0 1) with steps along ⟨1 0 0⟩, i.e. these steps are 100% kinked. They give a rough estimate for the interaction constant (62 meV Å); their value

is, however, based on the use of Eqs. (3) and (6) at $\theta = 0^\circ$, i.e. they did not make use of the real angle dependence of the step stiffness. Nevertheless, their result seems to be in agreement with our data (Fig. 9(b)).

Repulsive step–step interactions may arise from entropic repulsions [59] between steps as well as from elastic strain fields [60] at steps. If the step–step interaction potential is due to elastic lattice deformations, one interesting conclusion from our data in Fig. 9(b) is that kinks seem to considerably contribute to the elastic step–step interaction potential.

As a caveat we would finally like to emphasize that the step structure of real high-Miller-index surfaces may substantially deviate from the geometrically ideal surface structure. As has been shown in this work, thermally activated kinks may introduce a substantial number of kinks with mirror symmetry which could play an important role in enantioselective chemical reactions. At low temperatures though, thermally activated kinks may still be negligible compared to geometric kinks. As has been observed on Cu(5 8 90), however, the step orientation may deviate from the nominal direction in such a way that locally geometric kinks with mirror symmetry are dominant. A further point one should take into account when discussing the enantioselectivity of high-Miller-index substrates is the fact that reformation of the step profile may lead from steps with solely monoatomic long kinks to zig–zag steps with kinks of multi-atom length. The latter can be interpreted as straight step sections along a 90° rotated equivalent atomically dense direction. Hence, the number of chiral corners in the step profile would be substantially reduced in such a case.

5. Summary

In summary we have studied high-index steps on a vicinal surface to Cu(0 0 1) by STM. We have shown that the dominant mass transport on Cu(5 8 90) as used in our studies around room temperature is step edge diffusion. We find evidence for an influence of a kink–Ehrlich–Schwoebel barrier. Finally, we have demonstrated that the step–step interaction constant depends on the kink concentration. This could be evidence to a large contribution of geometric kinks to elastic lattice strain fields and elastic interaction potentials for Cu(1 0 0).

Acknowledgements

We acknowledge the high-accuracy sample preparation by Udo Linke. Furthermore, we have benefited from helpful discussion with Harald Ibach, Jülich, Joachim Krug, University of Essen and with Ted L. Einstein, University of Maryland. We thank Harald Ibach for the critical reading of the manuscript. This work was partially supported by the Fond der Chemischen Industrie, Germany.

References

[1] B. Lang, R.W. Joyner, G.A. Somorjai, Surf. Sci. 30 (1972) 454–474.
[2] G.A. Somorjai, R.W. Joyner, B. Lang, Proc. R. Soc. London Ser. A (Math. Phys. Sci.) 331 (1972) 335–346.
[3] S. Ferrer, J.M. Rojo, M. Salmeron, G.A. Somorjai, Philos. Mag. A (Phys. Condensed Matter Defects Mech. Properties) 45 (1982) 261–269.
[4] J. Perdereau, G.E. Rhead, Surf. Sci. 24 (1971) 555.
[5] D.W. Blakely, G.A. Somorjai, Surf. Sci. 65 (1977) 419–442.
[6] H. Ohtani, C.-T. Kao, M.A. Van Hove, G.A. Somorjai, Prog. Surf. Sci. 23 (1986) 155–316.
[7] C.C. Knight, G.A. Somorjai, Surf. Sci. 272 (1992) 326–333.
[8] E. Hahn, H. Schief, V. Marsico, A. Fricke, K. Kern, Phys. Rev. Lett. 72 (1994) 3378.
[9] T. Klas, R. Fink, G. Krausch, R. Platzer, J. Voigt, R. Wesche, G. Schatz, Europhys. Lett. 7 (1988) 151.
[10] G.A. Somorjai, M.A. Van Hove, Prog. Surf. Sci. 30 (1989) 201–231.
[11] J.C. Dunphy, C. Knight, P. Sautet, D.F. Ogletree, G.A. Somorjai, M.B. Salmeron, Surf. Sci. 280 (1993) 313–324.
[12] J.D. Batteas, J.C. Dunphy, G.A. Somorjai, M. Salmeron, Phys. Rev. Lett. 77 (1996) 534–537.
[13] M. Giesen, U. Linke, H. Ibach, Surf. Sci. 389 (1997) 264.
[14] X.-G. Zhang, M.A. Van Hove, G.A. Somorjai, P.J. Rous, D. Tobin, A. Gonis, J.M. MacLaren, K. Heinz, M. Michl, H. Lindner, K. Muller, M. Ehsasi, J.H. Block, Phys. Rev. Lett. 67 (1991) 1298–1301.
[15] M.A. Van Hove, G.A. Somorjai, Surf. Sci. 92 (1980) 489–518.
[16] G. Binnig, H. Rohrer, C. Gerber, Appl. Phys. Lett. 40 (1982) 178.
[17] G. Binnig, C.F. Quate, C. Gerber, Phys. Rev. Lett. 56 (1986) 930.
[18] J. Villain, D.R. Grempel, J. Lapujoulade, J. Phys. F 15 (1985) 809–834.
[19] J. Lapujoulade, Surf. Sci. Rep. 20 (1994) 191–250.
[20] H.-C. Jeong, E.D. Williams, Surf. Sci. Rep. 34 (1999) 171.
[21] M. Giesen, Prog. Surf. Sci. 68 (2001) 1.
[22] M. Giesen, C. Steimer, H. Ibach, Surf. Sci. 471 (2001) 80.
[23] G. Wulff, Z. Kristallgr. Mineral. 34 (1901) 449.
[24] M. Giesen-Seibert, H. Ibach, Surf. Sci. 316 (1994) 205.
[25] M. Giesen-Seibert, F. Schmitz, R. Jentjens, H. Ibach, Surf. Sci. 329 (1995) 47.
[26] M. Poensgen, J.F. Wolf, J. Frohn, M. Giesen, H. Ibach, Surf. Sci. 274 (1992) 430.
[27] C.F. McFadden, P.S. Cremer, A.J. Gellman, Langmuir 12 (1996) 2483.
[28] D.S. Sholl, Langmuir 14 (1998) 862.
[29] G.A. Attard, A. Ahmadi, J. Feliu, A. Rodes, E. Herrero, S. Blais, G. Jerkiewicz, J. Phys. Chem. B 103 (1999) 1381.
[30] A. Ahmadi, G. Attard, J. Feliu, A. Rodes, Langmuir 15 (1999) 2420.
[31] R.M. Hazen, D.S. Sholl, Nat. Mater. 2 (2003) 367.
[32] T.D. Power, A. Asthagiri, D.S. Sholl, Langmuir 18 (2002) 3737.
[33] A. Asthagiri, P.J. Feibelman, D.S. Sholl, Topics Catal. 18 (2002) 193.
[34] B. Poelsema, G. Comsa, Scattering of thermal energy atoms from disordered surfaces, in: Springer Tracts in Modern Physics, vol. 115, Springer, Berlin, 1989.
[35] S. Fölsch, G. Meyer, K.H. Rieder, M.H.-V. Hoegen, T. Schmidt, Surf. Sci. 394 (1997) 60.
[36] O. Pierre-Louis, Surf. Sci. 529 (2003) 114.
[37] S. Rousset, F. Pourmir, J.-M. Berroir, J. Klein, J. Lecoeur, P. Hecquet, B. Salanon, Surf. Sci. 422 (1999) 33–41.
[38] V.B. Shenoy, S. Zhang, W.F. Saam, Phys. Rev. Lett. 81 (1998) 3475.
[39] M. Giesen, M. Dietterle, D. Stapel, H. Ibach, D.M. Kolb, Surf. Sci. 384 (1997) 168.
[40] S. Baier, M. Giesen, H. Ibach, Surf. Sci., 2004.
[41] K. Besocke, Surf. Sci. 181 (1987) 145.
[42] J. Frohn, J.F. Wolf, K. Besocke, M. Teske, Rev. Sci. Instrum. 60 (1989) 1200.

[43] S. Dieluweit, H. Ibach, M. Giesen, T.L. Einstein, Phys. Rev. B 67 (2003) R121410(1–4).
[44] J.F. Wolf, B. Vicenzi, H. Ibach, Surf. Sci. 249 (1991) 233.
[45] M. Giesen-Seibert, R. Jentjens, M. Poensgen, H. Ibach, Phys. Rev. Lett. 71 (1993) 3521; 73 (1994) E911.
[46] M. Giesen-Seibert, R. Jentjens, M. Poensgen, H. Ibach, Phys. Rev. Lett. 73 (1994) E911.
[47] N.C. Bartelt, T.L. Einstein, E.D. Williams, Surf. Sci. 312 (1994) 411.
[48] A. Pimpinelli, J. Villain, D.E. Wolf, J.J. Métois, J.C. Heyraud, I. Elkinani, G. Uimin, Surf. Sci. 295 (1993) 143.
[49] S.V. Khare, T.L. Einstein, Phys. Rev. B 57 (1998) 4782.
[50] T. Ihle, C. Misbah, O. Pierre-Louis, Phys. Rev. B 58 (1998) 2289.
[51] E. LeGoff, L. Barbier, L. Masson, B. Salanon, Surf. Sci. 432 (1999) 139.
[52] B. Blagojevic, P.M. Duxbury, Phys. Rev. E 60 (1999) 1279.
[53] N.C. Bartelt, J.L. Goldberg, T.L. Einstein, E.D. Williams, Surf. Sci. 273 (1992) 252.
[54] M. Giesen, T.L. Einstein, Surf. Sci. 449 (2000) 191.
[55] G. Ehrlich, F.G. Hudda, J. Chem. Phys. 44 (1966) 1039.
[56] R.L. Schwoebel, E.J. Shipsey, J. Appl. Phys. 37 (1966) 3682.
[57] O. Pierre-Louis, M.R. D'Orsogna, T.L. Einstein, Phys. Rev. Lett. 82 (1999) 3661.
[58] S. Rousset, S. Gauthier, O. Siboulet, J.C. Girard, S.D. Cheveigné, M. Huerta-Garnica, W. Sacks, M. Belin, J. Klein, Ultramicroscopy 42–44 (1992) 515.
[59] B. Joós, T.L. Einstein, N.C. Bartelt, Phys. Rev. B43 (1991) 8153.
[60] V.I. Marchenko, A.Y. Parshin, Sov. Phys. JETP 52 (1981) 129.